
Are We Really Learning the Score Function? Reinterpreting Diffusion Models Through Wasserstein Gradient Flow Matching

Anonymous Author(s)

Affiliation

Address

email

Abstract

Diffusion models are commonly interpreted as learning the *score function*, i.e., the gradient of the log-density of noisy data. However, this assumption implies that the target of learning is a conservative vector field, which is not enforced by the neural network architectures used in practice. We present numerical evidence that trained diffusion networks violate both integral and differential constraints required of true score functions, demonstrating that the learned vector fields are not conservative. Despite this, the models perform remarkably well as generative mechanisms. To explain this apparent paradox, we advocate a new theoretical perspective: diffusion training is better understood as *flow matching* to the velocity field of a Wasserstein Gradient Flow (WGF), rather than as score learning for a reverse-time stochastic differential equation. Under this view, the “probability flow” arises naturally from the WGF framework, eliminating the need to invoke reverse-time SDE theory and clarifying why generative sampling remains successful even when the neural vector field is not a true score. We further show that non-conservative errors from neural approximation do not necessarily harm density transport. Our results advocate for adopting the WGF perspective as a principled, elegant, and theoretically grounded framework for understanding diffusion generative models.

1 Background

Diffusion models are typically described as follows: Given D -dimensional samples $x \in \mathbb{R}^D$ drawn from a data distribution μ_0 , one defines a forward Itô process that gradually corrupts x into noise. Throughout this paper, we use the continuous-time Ornstein–Uhlenbeck (OU) process for concreteness:¹

$$dX_t = -X_t dt + \sqrt{2} dW_t, \quad X_0 = x \sim \mu_0, \quad (1)$$

where each component of W_t is a standard Wiener process. The process (1) converges to a limiting distribution μ_∞ as $t \rightarrow \infty$, which is an isotropic Gaussian in \mathbb{R}^D . Because of the choice of diagonal matrices in the drift and diffusion terms, each component of X_t follows the well-studied one-dimensional OU process.

¹[16] established the equivalence of the OU process with the discrete-time Denoising Diffusion Probabilistic Model [10] and the score-based formulation [20]. This setup is often called “variance-preserving” (VP), though this term is misleading: for each sample, the variance is not constant over time (which, in most scientific contexts, is the definition of “preserving”), but grows as $\sqrt{1 - e^{-2t}}$. Our analysis extends naturally to the standard Brownian motion process $dX_t = dW_t$, commonly termed “variance-exploding” (VE).

28 Equivalently, the forward dynamics can be described in terms of densities. The transition kernel²
 29 $\rho(\xi, t | \zeta, s)$ satisfies the Fokker–Planck Equation (FPE):

$$\partial_t \rho(\xi, t | \zeta, s) = \nabla_\xi [\xi \rho(\xi, t | \zeta, s)] + \nabla_\xi^2 \rho(\xi, t | \zeta, s), \quad (2)$$

30 with the initial condition $\rho(\xi, 0) = \delta(\xi - x)$ for each of the drawn samples $x \sim \mu_0$, where $\delta(\cdot)$
 31 denotes the Dirac delta distribution.

32 The modern understanding of diffusion models is grounded in Anderson’s reverse-time theory [2],
 33 which guarantees the existence of a reverse-time Itô process that transforms samples from the simple
 34 distribution μ_∞ back into data-like samples as $t : \infty \rightarrow 0$:

$$dX_\tau = [X_\tau + 2s(X_\tau, -\tau)] d\tau + \sqrt{2} dW_\tau, \quad X_{-\infty} \sim \mu_\infty. \quad (3)$$

35 Here, we define $\tau := -t$, $\tau : -\infty \rightarrow 0$, $\rho(x, t)$ denotes the forward density with initial distribution
 36 μ_0 , $s(\xi, t) := \nabla_\xi \log \rho(\xi, t) \in \mathbb{R}^D$ is the score function of the corrupted (forward) distribution given
 37 initial distribution μ_0 , and dW_s is again a multi-dimensional Wiener process. The central training
 38 objective of diffusion models is thus framed as *learning the score function* $s(x, t)$ [20]. In practice, a
 39 neural network $\mathbb{R}^D \times \mathbb{R} \rightarrow \mathbb{R}^D$ is used to approximate $s(x, t)$, which is then plugged into (3) during
 40 sampling.

41 A key point is that the score function has a special mathematical structure: it is a conservative
 42 field. Neural networks used in practice are not constrained to produce conservative vector fields
 43 and, therefore, do not necessarily preserve this structure. This raises the central question of this
 44 study:

45 Does a trained neural network actually learn a valid *score function*, or merely a
 46 useful vector field for generative sampling?

47 1.1 Wasserstein Gradient Flow

48 Wasserstein Gradient Flow (WGF) originates from the theory of optimal transport (OT), but it has
 49 become increasingly relevant for understanding modern generative models. Here, we provide a brief
 50 overview and refer readers to the classic references [1, 7] for comprehensive materials.

51 Recall the forward evolution of the probability density $\rho(x, t)$ under the FPE (2). In their seminal
 52 work, Jordan, Kinderlehrer, and Otto observed that an implicit Euler discretization of the FPE can
 53 be reinterpreted as a variational problem: each timestep corresponds to minimizing a free energy
 54 functional that combines Shannon entropy with a Wasserstein-2 distance penalty [11]. This insight,
 55 known as the *JKO scheme*, shows that the FPE can be understood as a gradient flow of entropy in
 56 the space of probability measures.

57 Building on this idea, Otto introduced a formal Riemannian calculus on the space of probability dis-
 58 tributions, demonstrating that the FPE defines a steepest descent in Wasserstein geometry [15]. This
 59 framework—now widely known as Otto calculus—precisely formalizes the notion that probability
 60 densities evolve like particles sliding down an energy landscape, but within the geometry induced by
 61 optimal transport. In addition, Otto also introduced the generalized Liouville equation (GLE)³[9].
 62 Taken together, the JKO scheme and Otto’s formulation provide the foundation for WGF, unifying
 63 PDE evolution, entropy maximization, and optimal transport. One powerful result of WGF theory
 64 is:

65 While the sample paths of the diffusion process that FPE describes are fundamen-
 66 tally *stochastic*, the marginal distribution⁴ of the paths at a specific time, $\rho(\cdot, t)$, is
 67 identical to the marginal distribution of the trajectories driven by a deterministic
 68 WGF.

²Since the OU process decomposes into D independent one-dimensional processes, the density factorizes across coordinates: $\rho(\xi, t | \zeta, s) = \prod_{i=1}^D \rho_i(\xi_i, t | \zeta_i, s)$

³We distinguish GLE from the “continuity equation”, a term commonly used in the field of OT. We make this distinction because continuity equations in physics can describe arbitrary conserved quantities (mass, energy, etc.), but the GLE specifically governs normalized probability density functions.

⁴ $\rho(\cdot, t)$ is referred to as the marginal distribution because it is only the distribution of X_t at time t . It is a marginal distribution of the the joint distribution specified the stochastic process, $\rho(x_{t_1}, \dots x_{t_N})$.

69 To see this, let us consider setting the energy functional as the sum of a quadratic potential and the
70 negative Shannon entropy

$$E \{ \rho(\cdot, t) \} := \int \frac{x^2}{2} \rho(x, t) dx + \int \rho(x, t) \log \rho(x, t) dx. \quad (4)$$

71 Here, the first term accounts for the drift/advection and the second for the diffusion in the FPE (2).
72 The idea is to identify the *steepest descent* direction functions that decrease the energy the most in
73 the space of probability density functions induced by a deterministic velocity field $v(x, t)$. Applying
74 d/dt to the energy functional:

$$\frac{d}{dt} E \{ \rho(\cdot, t) \} = \int \frac{\delta E \{ \rho(\cdot, t) \}}{\delta \rho(x, t)} \frac{\partial \rho(x, t)}{\partial t} dx, \quad (5)$$

75 where the functional variation of E with respect to the density function ρ can be explicitly computed:

$$\begin{aligned} \frac{\delta E \{ \rho(\cdot, t) \}}{\delta \rho(x, t)} &:= \frac{1}{\delta \rho(x, t)} \left[\int \frac{x^2}{2} \delta \rho(x, t) + (\rho + \delta \rho) \log(\rho + \delta \rho) dx - \int \rho(x, t) \log \rho(x, t) dx \right] \\ &\sim \frac{1}{\delta \rho(x, t)} \int \left[\frac{x^2}{2} + \log \rho(x, t) + 1 \right] \delta \rho(x, t) dx = \frac{x^2}{2} + \log \rho(x, t). \end{aligned} \quad (6)$$

76 In the last two equations, we neglected higher-order $\mathcal{O}(\delta \rho(x, t))$ terms (using the asymptotic sym-
77 bol \sim) and applied the normalization condition that the functional perturbation $\int \delta \rho(x, t) dx = 0$
78 because $\int \rho(x, t) dx = 1 = \int (\rho + \delta \rho)(x, t) dx$. Next, inserting GLE [9] (see footnote 3):

$$\partial_t \rho(x, t) = -\nabla_x \cdot [v(x, t) \rho(x, t)], \quad (7)$$

79 and the functional variation (6) into (5) leads to

$$\begin{aligned} \frac{d}{dt} E \{ \rho(\cdot, t) \} &= - \int \left[\frac{x^2}{2} + \log \rho(x, t) \right] \nabla_x \cdot [v(x, t) \rho(x, t)] dx \\ &= \int v(x, t) \cdot [x + \nabla_x \log \rho(x, t)] \rho(x, t) dx, \end{aligned} \quad (8)$$

80 where we used integration by parts and assumed vanishing boundary terms. The above equation
81 can be interpreted as an inner product of the functions $v(\cdot, t)$ and $\nabla_x \log \rho(\cdot, t)$ under the measure
82 $\rho(\cdot, t)$. Clearly, the velocity field that corresponds to the steepest descent of the energy functional
83 should align with the opposite direction of $\nabla_x \log(\cdot, t)$ (up to a global multiplicative constant):

$$v_{\text{WGF}}(x, t) := -x - \nabla_x \log \rho(x, t) = -x - s(x, t). \quad (9)$$

84 The probability distribution of the resulting flow system with the above velocity field evolves under
85 the GLE:

$$\frac{\partial}{\partial t} \rho(x, t) = -\nabla_x \cdot [v_{\text{WGF}}(x, t) \rho(x, t)] = \nabla_x [(x + \nabla_x \log \rho(x, t)) \rho(x, t)], \quad (10)$$

86 which is exactly the FPE (2) describing the OU.

87 Song et al. rediscovered the WGF velocity field (9) through manipulating the FPE and noticing
88 $\nabla_x \rho(x, t) = \rho(x, t) \nabla_x \log \rho(x, t)$. They used the term “probability flow”, without referencing the
89 JKO scheme, Otto calculus, and WGF. We believe it is beneficial to point out the origin of this
90 theoretical framework, given its deeper connection to OT and the variational nature of the diffusion
91 process.

92 2 Numerical experiments

93 We now shift our focus to numerical experiments to verify the central question we have in score-
94 based generative modeling: *Are we learning the score function?*

95 Due to the definition of the score function, $s(x, t) := \nabla_x \log \rho(x, t)$, the fundamental theorem of
96 calculus (or generalized Stokes’ theorem in high dimension) states that the line integral of the score
97 function along a closed path in the state space has to be equal to zero:

$$\oint \vec{s}(x, t) \cdot d\vec{x} = 0. \quad (11)$$

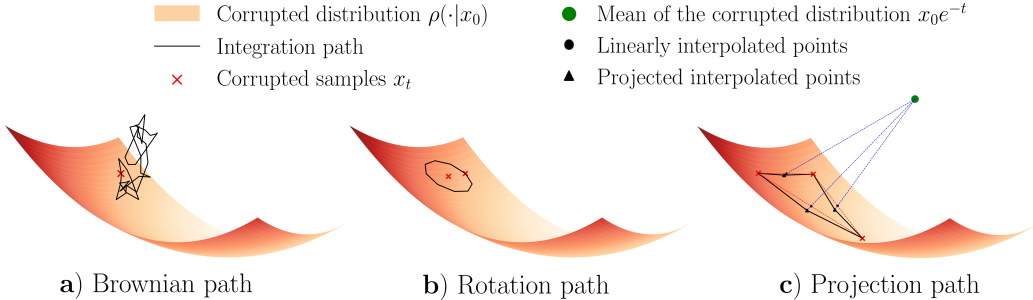


Figure 1: Mechanisms for assessing integral constraints. Illustration of the three mechanisms we used to construct closed paths for evaluating integral constraints within the high-density regions of the data distribution.

98 We will refer to (11) as the *integral constraint*. The second constraint, also following directly from
 99 the definition of the score function, states:

$$\frac{\partial}{\partial x_j} s_i(x, t) = \frac{\partial}{\partial x_i} s_j(x, t), \quad \text{for any pair } (i, j) \in \{1 \dots D\}^2. \quad (12)$$

100 We refer to (12) as the *differential constraint*. Our goal is to numerically investigate whether either of
 101 the constraints are met in trained diffusion models.

102 2.1 Models and datasets

103 To present a minimal working example, we trained a MNIST diffusion model using a lightweight
 104 U-Net implementation. The model is composed of ShuffleNet-style residual bottlenecks and depth-
 105 wise convolutions. The time indices are embedded, passed through an MLP, and added to the feature
 106 maps in each block. It employs simple encoder-decoder blocks with downsampling and upsampling
 107 and skip connections, keeping the model lightweight (around 4 MB). The implementation can be
 108 found at [3]. We used the cosine schedule [14] and a total discrete time index $T = 1000$, which
 109 corresponds to observing time-homogeneous OU process (1) at discrete times [16]

$$t_k = -\frac{1}{2} \log \frac{f(k)}{f(0)}, \quad f(k) := \cos \left(\frac{k/T + 0.008 \pi}{1 + 0.008} \frac{\pi}{2} \right) \quad (13)$$

110 We also performed the same test with latent diffusion, using a VAE with an 8×8 latent space
 111 (implementation based on [18]). The diffusion process employs the same network as before but acts
 112 in the latent space of the VAE.

113 The purpose of this experiment is to enable a comprehensive analysis with tractable computation,
 114 especially for evaluating the differential constraints. The results are presented in the following
 115 sections. We also observed a similar behavior for the CIFAR-10 dataset (Appendix 4.2).

116 2.2 Integral constraints

117 To numerically check the integral constraint (11), we introduce three different mechanisms for gen-
 118 erating closed paths on which the integral is evaluated:

119 • **Brownian path.** Starting from a corrupted sample $x_t \in \mathbb{R}^D$ generated by the forward diffusion,
 120 we perform a random walk on \mathbb{R}^D using a Brownian bridge, which generates a path in \mathbb{R}^D starting
 121 and ending at x_t . The path of Brownian bridge is $X_u^{\text{BB}} = W_u - uW_U/U$ with a fictitious time
 122 $u \in [0, U]$. We choose $U = 9$, uniformly sample 1,000 discrete time steps in between, and add
 123 the resulting path to a forward sample x_t , i.e., $y_{u,t} = x_t + X_u^{\text{BB}}$. This method does not guarantee
 124 that the path stays close to the typical region induced by the forward process, as illustrated in
 125 Fig. 1 (a). We include this path as a way to study the behavior of out-of-distribution samples.

126 • **Rotation path.** Following the typical application of image corruption process, the corrupted
 127 sample $x_t = x_0 e^{-t} + \sqrt{1 - e^{-2t}} \varepsilon$, where $\varepsilon \sim \mathcal{N}(0, I)$. We randomly pair each of the D

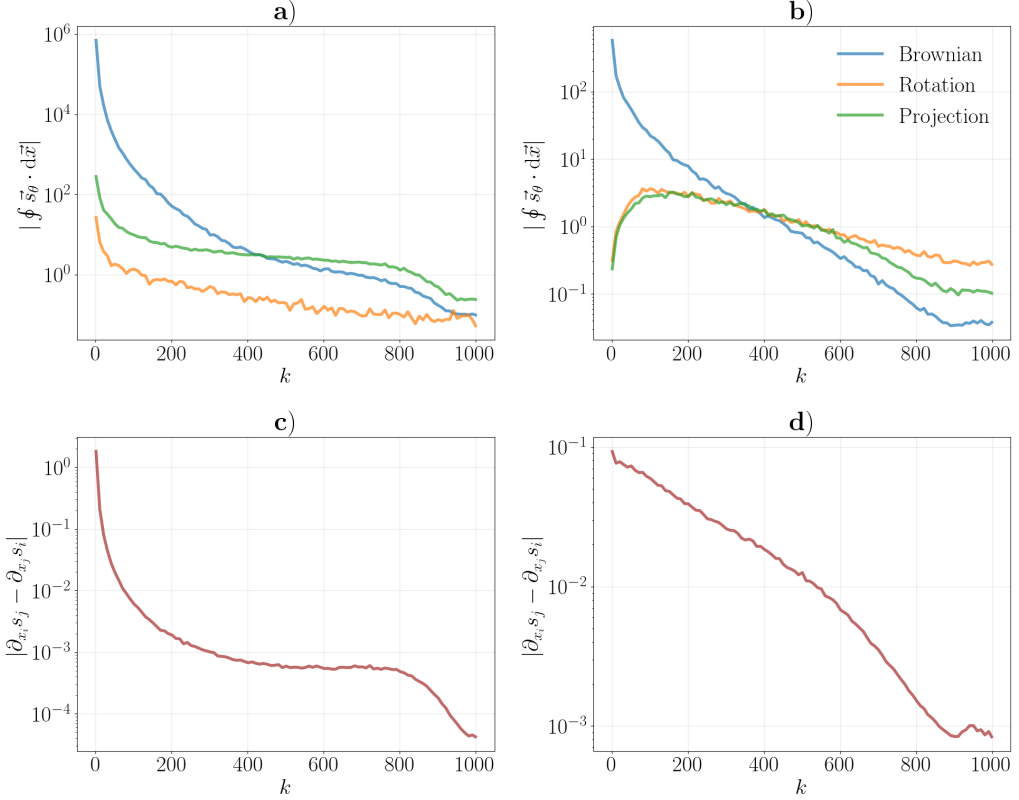


Figure 2: Results of integral and differential constraints, as functions of discrete time index k : **a**) shows the absolute value of the integral condition $|\oint \vec{s}_\theta \cdot d\vec{x}|$; **b**) presents the same quantity but for the latent dynamics; **c**) reports the differential condition $|\partial_{x_i} s_j - \partial_{x_j} s_i|$ in normal diffusion; **d**) shows the corresponding differential condition in latent diffusion.

128 components of ε , so $(\varepsilon_i, \varepsilon_j)$ forms a two-dimensional vector. Then, we rotate each of the $D/2$
129 two-dimensional vectors with respect to the origin, i.e., $\varepsilon'_i(u) = \cos(2\pi u)\varepsilon_i + \sin(2\pi u)\varepsilon_j$ and
130 $\varepsilon'_j(2\pi u) = -\sin(2\pi u)\varepsilon_i + \cos(2\pi u)\varepsilon_j$. Note that we rotate all $D/2$ pairs with the same “angular
131 velocity”. The resulting vector is used to generate a closed loop in the x -space, i.e., $y_{u,t} = x_0 e^{-t} +$
132 $\sqrt{1 - e^{-2t}} \varepsilon'(u)$, $u : 0 \rightarrow 1$. With this construct, the probability density of noise realization $\varepsilon'(u)$
133 is identical to that of the original noise realization ε , ensuring the closed path in the x -space sits
134 in the region where most of the probability mass is.

135 **• Projection path.** We first generate multiple corrupted samples x_t from the same initial x_0 , then
136 find a way to connect these points such that the connections lie in the typical set of corrupted
137 distribution. In order to achieve this, we propose a simple mechanism: to connect two corrupted
138 samples x_t and x'_t , we first generate points that linearly interpolate between the two samples, and
139 then project the interpolated points back to the corrupted distribution. Since Gaussian diffusion
140 in high-dimensional space induces the structure of a thin shell around the clean samples, the
141 projection can be carried out by projecting the samples radially back to the shell in \mathbb{R}^D , whose
142 radius is estimated either through Monte Carlo sampling (which we also know would be $\approx \sqrt{D}$
143 from asymptotic analysis). An illustrative schematic diagram is provided in Fig. 1 (c).

144 Figures 2 (a) and (b) show the results of evaluating the integral constraint using these three methods
145 of generating closed paths. Summary statistics of these distributions are provided in Fig. 4 in the
146 Appendix.

147 Clearly, the integral condition is not satisfied in the trained neural network. One may argue whether
148 the magnitude matters to the reverse-time dynamics. To answer this, we notice that the score-induced

149 drift $2s(x, t)$ is added to a linear term $x(t)$ in (3); this provides us a non-dimensional quantity:

$$\frac{2 \oint \vec{s}(\vec{y}, t) \cdot d\vec{y}}{\oint |\vec{y}| |d\vec{y}|}, \quad (14)$$

150 where \vec{y} is a dummy vector looping over the generated path. Results of this quantity are presented
151 in Figs. 5 and 6 in Appendix, showing a significant deviation from 0.

152 **2.3 Differential constraints**

153 Due to the intensive resources required to compute the full Jacobian matrix, we instead randomly
154 sample 64 components of the predicted score $s(x, t)$ and 64 components of the corrupted samples
155 x_t to compute a 64×64 sub-Jacobian matrix. The statistics were collected from 256 samples for
156 each time step, and are presented in Fig. 2 (c) and (d), both showing non-zero contributions.

157 **3 Discussion**

158 The numerical evidence clearly suggests that *the trained neural network does not learn the score*
159 *function*, which is a conservative field. However, the trained network can definitely perform the
160 generative task. The observation raises an interesting question: what is the trained neural network
161 actually learning in order to perform the generative task?

162 We here propose a bold hypothesis, leveraging the WGF theory, to understand what happens in the
163 “score-matching” generative modeling. Our assertion is:

164 Existing diffusion modeling is better understood as modeling a normalizing flow
165 [5], through performing flow matching [12] to the WGF velocity (9), rather than
166 learning the reverse stochastic differential equation established by [2], popularized
167 by [20].

168 Contrary to typical flow-based models [5] which learn the velocity field by maximizing the end-
169 to-end likelihood, the flow-matching method [12] matches the neural velocity field to a target ve-
170 locity field. The target velocity field is often analytically derived for a prescribed transport from
171 the data distribution to an easy-to-sample distribution (often isotropic Gaussian distribution in high
172 dimension), and evaluated on sampled training data. Here, we use the WGF induced by the energy
173 functional (4) as the prescribed transport, and match the velocity field (9). More precisely, we only
174 match the flow induced by the entropic term in (4).

175 There are several advantages to understand the diffusion model as the flow-matching WGF. First, the
176 “probability flow” is naturally included in the WGF framework. Secondly, we can formally bypass
177 the necessity to invoke the reverse-time Itô process, which can be confusing and counterintuitive—
178 as will be seen below, within the WGF and Otto calculus framework, the deterministic probability
179 flow ODE arises naturally, bypassing the need to explicitly route through Anderson’s reverse-time
180 SDE. Finally, flow-matching WGF naturally explains why the trained neural flow, which fails to
181 obey the differential and integral score conditions, can still perform in generative modeling.

182 To see this, let us illustrate a self-consistent narrative of a flow-matching problem:

183 1. **Optimization objective.** Our goal is to learn (9) through flow-matching. We choose to minimize
184 the L^2 error between the neural velocity and the entropy-induced velocity field in (9)

$$\min_{\theta} \mathbb{E}_{k \sim \text{Unif}(\{1, 2, \dots, T\})} \mathbb{E}_{x \sim \rho(\cdot, t)} \|v_{\theta}(\cdot, t_k) - s(\cdot, t_k)\|_2 \quad (15)$$

185 2. **Data generation.** Samples to perform Monte Carlo approximation of the above L^2 -norm will
186 be drawn from the distribution at time t , induced by the energy function (4). Instead of using
187 the WGF in the forward dynamics, which involves estimating $\log \rho$ in high dimension, we use
188 the equivalent OU process (1) to generate sample and more importantly, to compute *analytically*
189 *exact* $s(x, t)$ for matching the neural velocity field.

190 3. **Sampling/Inference.** To perform the generative task, terminal samples drawn from the isotropic
191 Gaussian are transported from $t \rightarrow \infty$ to $t = 0$ by integrating the ordinary differential equation
192 backward in time. That is, $dx(\tau)/d\tau = -v_{\text{WGF}}(x(\tau)) = x(\tau) + \text{NN}(x(\tau), -\tau)$, where $\tau \equiv -t$,

193 so signs flip relative to forward time. $x(\infty) \sim \mathcal{N}(0, I)$ and $\tau : -\infty \rightarrow 0$. The corresponding
194 GLE [9] is

$$\frac{\partial}{\partial \tau} \rho(x, t) = -\nabla_x [(x + v_{\theta^*}(x, -\tau)) \rho(x, t)], \quad (16)$$

195 where θ^* stands for the trained neural weights.

196 Operationally, the above descriptions are identical to applying the “score-matching” for training and
197 performing “probability flow” for inference [20]. However, because of the deterministic nature of
198 the WGF, we would not need to invoke the reverse-time stochastic process [2]. The simplicity is the
199 first benefit of recognizing the existing approach as a Wasserstein Gradient Flow-Matching problem.

200 By framing the learning as a flow-matching problem, it is most natural to weight each time equally,
201 which is the *de facto* training procedure for both discrete-time [10] and continuous-time [20] diffu-
202 sion models. The procedure would seem *ad hoc* if one aims to parameterize a neural network for
203 learning the reverse-time diffusion process by a more theoretically grounded log-likelihood (more
204 precisely, the bound of which) maximization as shown in [19]. As DDPM [10] pointed out, the log-
205 likelihood approach involved weights which are not uniform in time; by removing such non-uniform
206 weights, DDPM achieved a better performance by effectively solving a flow-matching problem.

207 Next, assuming that we learn the WGF perfectly, we can treat the reverse-time WGF as a dynamical
208 system:

$$\frac{d}{d\tau} x(\tau) = x(\tau) + \text{NN}(x(\tau), -\tau) = x(\tau) + \nabla_x \log(x(\tau), -\tau). \quad (17)$$

209 This system is identical to a Wasserstein Gradient Flow with the energy functional,

$$\begin{aligned} E\{\rho(\cdot, \tau)\} &= - \int \frac{x^2}{2} \rho(x, \tau) dx - \int \rho(x, s) \log \rho(x, \tau) dx \\ &= - \underbrace{\int \frac{x^2}{2} \rho(x, \tau) dx}_{\text{Reverse-time drift}} - 2 \underbrace{\int \rho(x, \tau) \log \rho(x, \tau) dx}_{\text{Reverse-time diffusion}} + \underbrace{\int \rho(x, \tau) \log \rho(x, \tau) dx}_{\text{Reverse-time diffusion}} \end{aligned} \quad (18)$$

210 which is equivalent to the reverse-time Itô process (3). This suggests that we would not need to in-
211 voke Anderson’s seminal proof of the existence of the reverse diffusion [2] for generative task. This
212 justifies the second advantage of the WGF framework. We remark, however, that to rigorously estab-
213 lish the equivalence of the forward and reverse *path measures*, Anderson’s theory remains necessary.
214 Nevertheless, because generative diffusion models only require consistency at the level of marginal
215 densities, it is not necessary to invoke path measures in practice. We emphasize that our results con-
216 cern density transport (marginals). We do not make claims about sample-path equivalence, which
217 requires Anderson’s reverse-time construction. However, the corresponding reverse-time Itô process
218 not only can be used as a stochastic process for sampling, but also coincidentally the reverse-time
219 process established by Anderson [2].

220 Finally, as suggested by our numerical analysis, the neural network is *not* learning a gradient of
221 a scalar potential, i.e. $\text{NN}(x, t) \neq s(x, t)$ for all t , both globally (because it violates the integral
222 conditions) or locally (because it violates the differential conditions.) It is thus puzzling and chal-
223 lenging to analyze how the violations affect the reverse-time diffusion, and consequently the quality
224 of the generated samples. The flow representation can bring some insight here. Suppose we use
225 the trained, yet imperfect neural velocity field $\text{NN}(x, t) \approx \nabla_x \log \rho(x, t)$. Denote the error by
226 $e(x, t) := s(x, t) - \text{NN}(x, t)$. Then, the GLE governing the distribution driven by the neural veloc-
227 ity field is

$$\begin{aligned} \frac{\partial}{\partial \tau} \rho(x, \tau) &= - \frac{\partial}{\partial x} [(x + \text{NN}(x, -\tau)) \rho(x, -\tau)] \\ &= - \frac{\partial}{\partial x} [(x + s(x, -\tau)) \rho(x, -\tau)] + \frac{\partial}{\partial x} [e(x, -\tau) \rho(x, -\tau)] \\ &= - \frac{\partial}{\partial x} [(x + s(x, -\tau)) \rho(x, -\tau)] \\ &\quad + [\nabla_x \cdot e(x, -\tau) + s^T(x, -\tau) \cdot e(x, -\tau)] \rho(x, -\tau). \end{aligned} \quad (19)$$

228 Immediately, we can identify a condition that if the error field $e(x, t)$ satisfies

$$0 = \nabla_x \cdot e(x, t) + s^T(x, t) \cdot e(x, t), \quad (20)$$

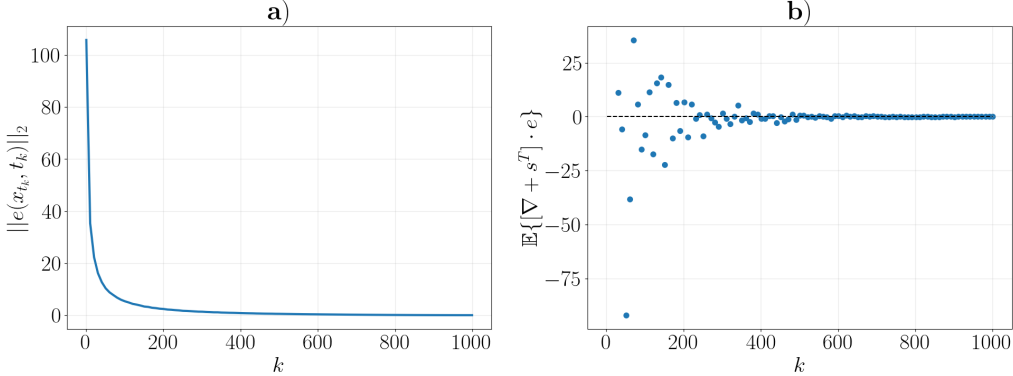


Figure 3: **a)** L2 norm of $e(x, t)$ and **b)** Stein operator value of $e(x, t)$.

229 the induced distribution is identical to the true distribution. In other words, if $e(x, t)$ lives in the
 230 null kernel of the operator $\nabla_x + s^T(x, t)$, the trained neural network can perfectly perform the
 231 generative task, even if it is not perfectly capturing the score function. We remark that this vector
 232 operator is related to the Stein operator [13] and is the key construct in several recent papers on
 233 sampling [4, 6, 21]. In Fig. 3, we computed the error field on a trained latent diffusion model using
 234 forward generated samples, showing that indeed a significant $e(x, t)$ is induced (which is of order
 235 10^2 , significant compared to the order 10^0 of deterministic decaying flow, $\dot{x}(t) = -x(t)$), but the
 236 error field is statistically confined⁵ in the null kernel. This analysis suggests that:

237 Even when $\text{NN}(x, t)$ is not the score function $\nabla_x \log p(x, t)$, the trained neural
 238 network can still be effective to perform generative modeling.

239 We remark that this analysis is only possible by recognizing the underlying flow structure. We
 240 humbly acknowledge that we are not the first to propose the equivalence between diffusion and flow
 241 models: Song et al. [20] recognized the ‘‘probability flow/ODE’’ and even suggested density and
 242 likelihood estimation, and very recently, Gao et al. pointed out the resemblance between diffusion
 243 and flow models [8]. Nevertheless, to our best knowledge, there have been no studies connecting
 244 diffusion models and normalizing flow parametrized by flow matching through the elegant theory of
 245 WGF and Otto calculus. The existing theories neither connect the flow operator to the Stein operator
 246 [13]. Furthermore, the identification of a unified description between the diffusion models and WGF
 247 could inspire new forward random sampling (‘‘data generation’’) for training and regularizing flow-
 248 based models.

249 To conclude, we advocate for this theoretical framework because, first, it was developed over 20
 250 years ago, and yet has been largely ignored in the machine learning literature, and second, the setup
 251 is self-consistent, simple, concise, and elegant. We dedicate this work to the pioneers of WGF
 252 theory—Jordan, Kinderlehrer, and Otto—whose foundational insights continue to shape and inspire
 253 cutting-edge machine learning research today.

254 References

- 255 [1] Luigi Ambrosio, Nicola Gigli, and Giuseppe Savaré. *Gradient Flows: In Metric Spaces and*
 256 *in the Space of Probability Measures*. 2nd ed. Basel: Birkhäuser, 2008. ISBN: 978-3-7643-
 257 8722-8.
- 258 [2] Brian D.O. Anderson. ‘‘Reverse-time diffusion equation models’’. en. In: *Stochastic Processes*
 259 *and their Applications* 12.3 (May 1982), pp. 313–326. ISSN: 03044149. DOI: 10 . 1016 /
 260 0304-4149(82)90051-5.
- 261 [3] bot66. *MNISTDiffusion: Implement a MNIST (also minimal) version of denoising diffusion*
 262 *probabilistic model from scratch*. <https://github.com/bot66/MNISTDiffusion>. 2022.

⁵We averaged over 256 randomly generated forward samples x_t . For each sample, the sufficient condition does not seem to be met but the average seems to agree, noting the significant variance for small k .

263 [4] Peng Chen and Omar Ghattas. *Projected Stein Variational Gradient Descent*. June 2020.
 264 arXiv: 2002.03469 [cs].

265 [5] Ricky T. Q. Chen et al. *Neural Ordinary Differential Equations*. Dec. 2019. arXiv: 1806 .
 266 07366 [cs, stat].

267 [6] Mingzhou Fan et al. “Path-Guided Particle-based Sampling”. In: *Proceedings of the 41st*
 268 *International Conference on Machine Learning*. PMLR, July 2024, pp. 12916–12934.

269 [7] Alessio Figalli and Federico Glaudo. *An Invitation to Optimal Transport, Wasserstein Dis-*
 270 *tances, and Gradient Flows*. Second edition. Berlin, Germany: EMS Press, 2023. ISBN: 978-
 271 3-98547-550-6.

272 [8] Ruiqi Gao et al. “Diffusion Models and Gaussian Flow Matching: Two Sides of the Same
 273 Coin”. In: *The Fourth Blogpost Track at ICLR 2025*. Feb. 2025.

274 [9] G. Gerlich. “Die verallgemeinerte Liouville-Gleichung”. en. In: *Physica* 69.2 (Nov. 1973),
 275 pp. 458–466. ISSN: 0031-8914. DOI: 10.1016/0031-8914(73)90083-9.

276 [10] Jonathan Ho, Ajay Jain, and Pieter Abbeel. *Denoising Diffusion Probabilistic Models*.
 277 Dec. 16, 2020. arXiv: 2006.11239 [cs, stat].

278 [11] Richard Jordan, David Kinderlehrer, and Felix Otto. “The Variational Formulation of the
 279 Fokker–Planck Equation”. In: *SIAM Journal on Mathematical Analysis* 29.1 (Jan. 1998),
 280 pp. 1–17. ISSN: 0036-1410. DOI: 10.1137/S0036141096303359.

281 [12] Yaron Lipman et al. “Flow Matching for Generative Modeling”. en. In: Sept. 2022. URL:
 282 <https://openreview.net/forum?id=PqvMRDCJT9t>.

283 [13] Qiang Liu and Dilin Wang. “Stein Variational Gradient Descent: A General Purpose Bayesian
 284 Inference Algorithm”. In: *Advances in Neural Information Processing Systems*. Ed. by D. Lee
 285 et al. Vol. 29. Curran Associates, Inc., 2016.

286 [14] Alex Nichol and Prafulla Dhariwal. *Improved Denoising Diffusion Probabilistic Models*.
 287 Feb. 18, 2021. arXiv: 2102.09672 [cs, stat].

288 [15] Felix Otto. “The Geometry of Dissipative Evolution Equations: The Porous Medium Equa-
 289 tion”. In: *Communications in Partial Differential Equations* 26.1-2 (2001), pp. 101–174. DOI:
 290 10.1081/PDE-100002243.

291 [16] Javier E. Santos and Yen Ting Lin. *Understanding Denoising Diffusion Probabilistic Models*
 292 *and their Noise Schedules via the Ornstein–Uhlenbeck Process*. Oct. 2023. arXiv: 2311 .
 293 17673 [stat,cond-mat, cs,math-ph].

294 [17] Won Seong. *Simple Latent Diffusion Model*. <https://huggingface.co/spaces/JuyeopDang/KoFace-AI>. 2024.

295 [18] sksq96. *A CNN Variational Autoencoder in PyTorch*. <https://github.com/sksq96/pytorch-vae/blob/master/vae.py>. 2018.

296 [19] Jascha Sohl-Dickstein et al. *Deep Unsupervised Learning Using Nonequilibrium Thermody-
 297 namics*. Nov. 18, 2015. arXiv: 1503.03585 [cond-mat, q-bio, stat].

298 [20] Yang Song et al. *Score-Based Generative Modeling through Stochastic Differential Equa-
 299 tions*. Comment: ICLR 2021 (Oral). Feb. 10, 2021. arXiv: 2011.13456 [cs, stat].

300 [21] Yifeng Tian, Nishant Panda, and Yen Ting Lin. “Liouville Flow Importance Sampler”. In:
 301 *Forty-First International Conference on Machine Learning*. June 2024.

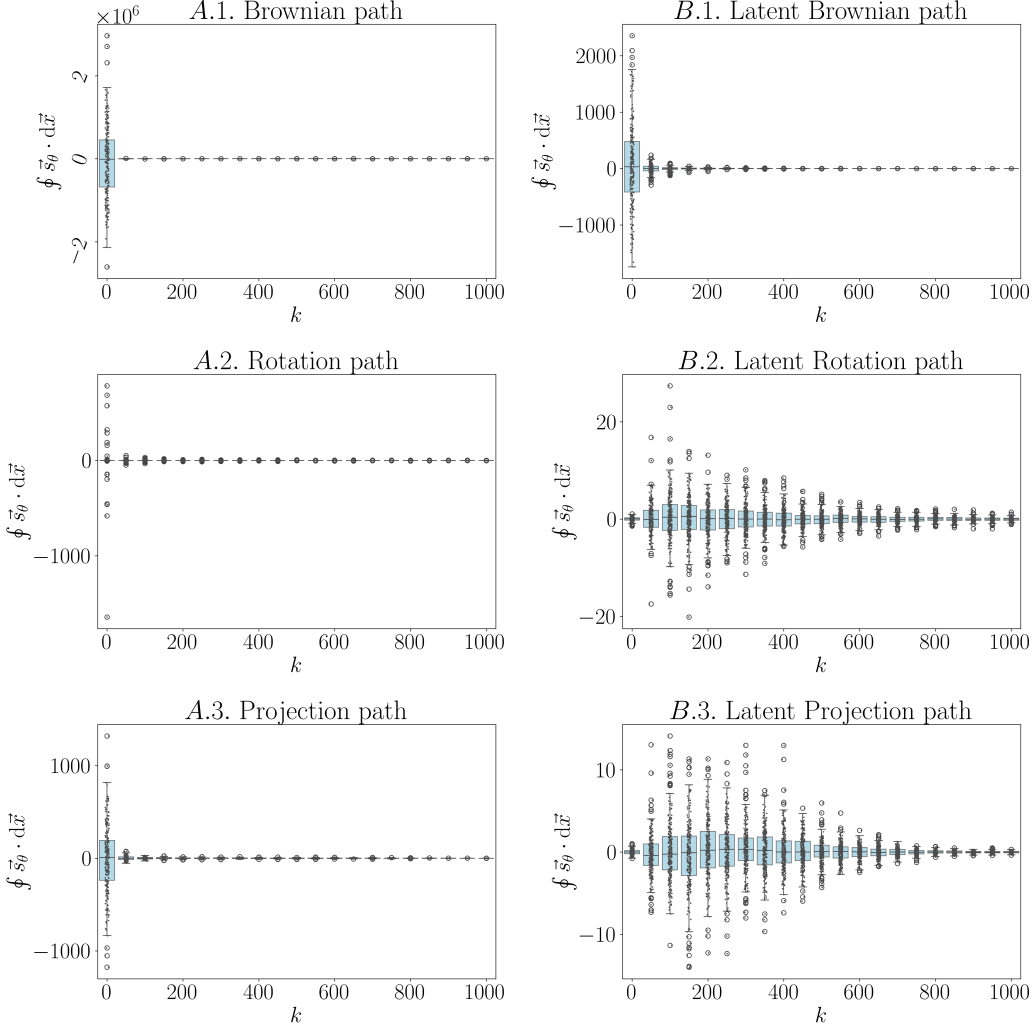


Figure 4: (MNIST) Summary statistics of $\oint \vec{s}_\theta \cdot d\vec{x}$ calculated by different path-generating mechanisms, in normal and latent diffusions.

304 4 Appendix

305 We provide more statistics of the non-dimensionalized quantity $|\oint \vec{s}_\theta d\vec{x}| / \oint |\vec{x}_t| \cdot |d\vec{x}|$ (14), as well
 306 as experiment results on the CIFAR-10 dataset.

307 4.1 More numerical results on MNIST

308 Refer to Figs. 4, 5, 6.

309 4.2 Numerical results on CIFAR-10

310 For CIFAR-10, we utilized the models from [17], it implements the standard DDPM and VAE with
 311 latent dimension of $3 \times 16 \times 16$. We also tried training these models from scratch, which exhibits
 312 similar behaviors to the pretrained ones. Results are presented in Figs. 7, 8, 9, 10.

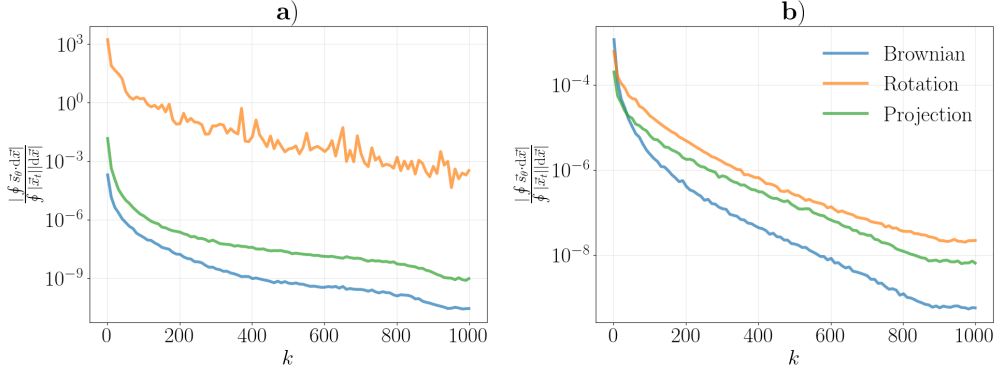


Figure 5: (MNIST) Results of integral constraints, as functions of discrete time index k : **a)** shows the absolute value of the integral condition $\int \vec{s}_\theta \cdot d\vec{x}$ normalized by the path length and the strength of the deterministic flow, $\int |\vec{x}_t| |d\vec{x}|$; **b)** presents the same quantity but for the latent dynamics.

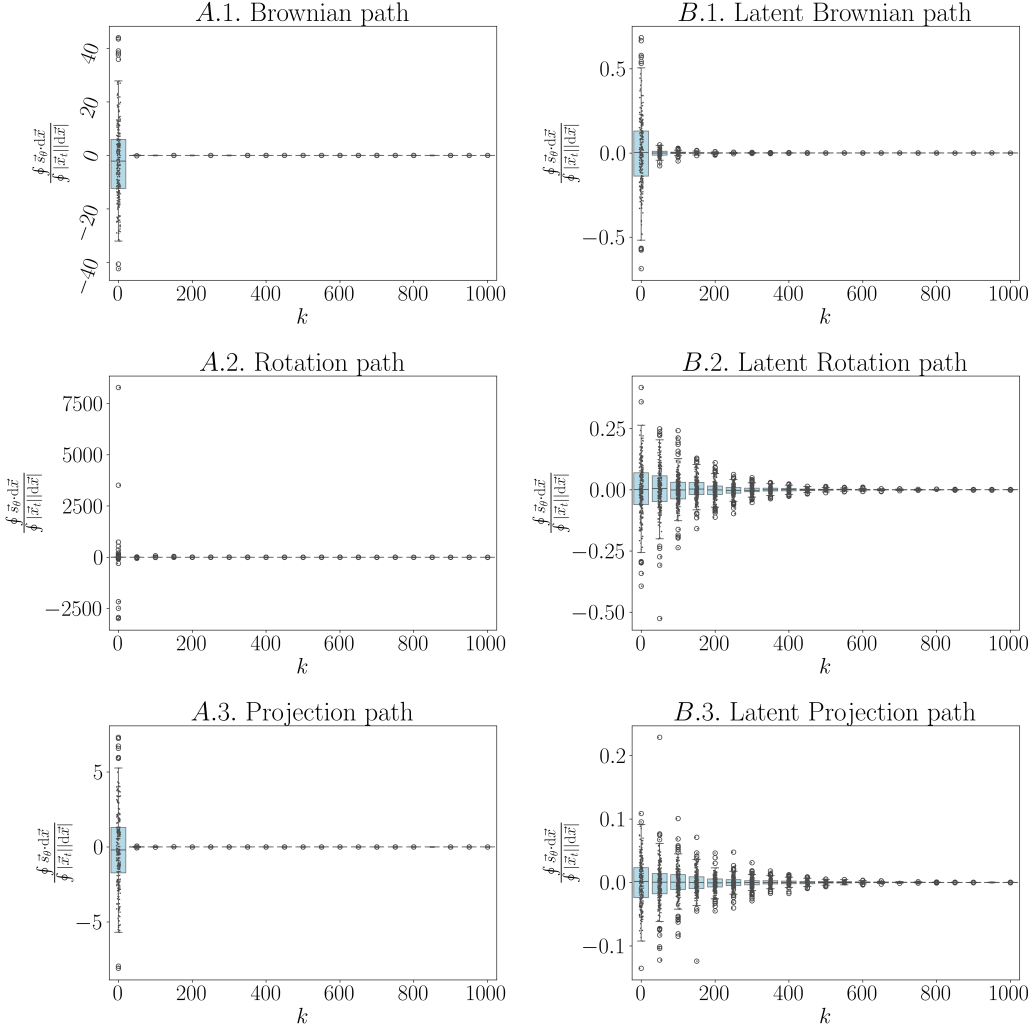


Figure 6: (MNIST) Summary statistics of $|\int \vec{s}_\theta \cdot d\vec{x}| / \int |\vec{x}_t| |d\vec{x}|$ calculated by different path-generating mechanisms, in normal and latent diffusions.

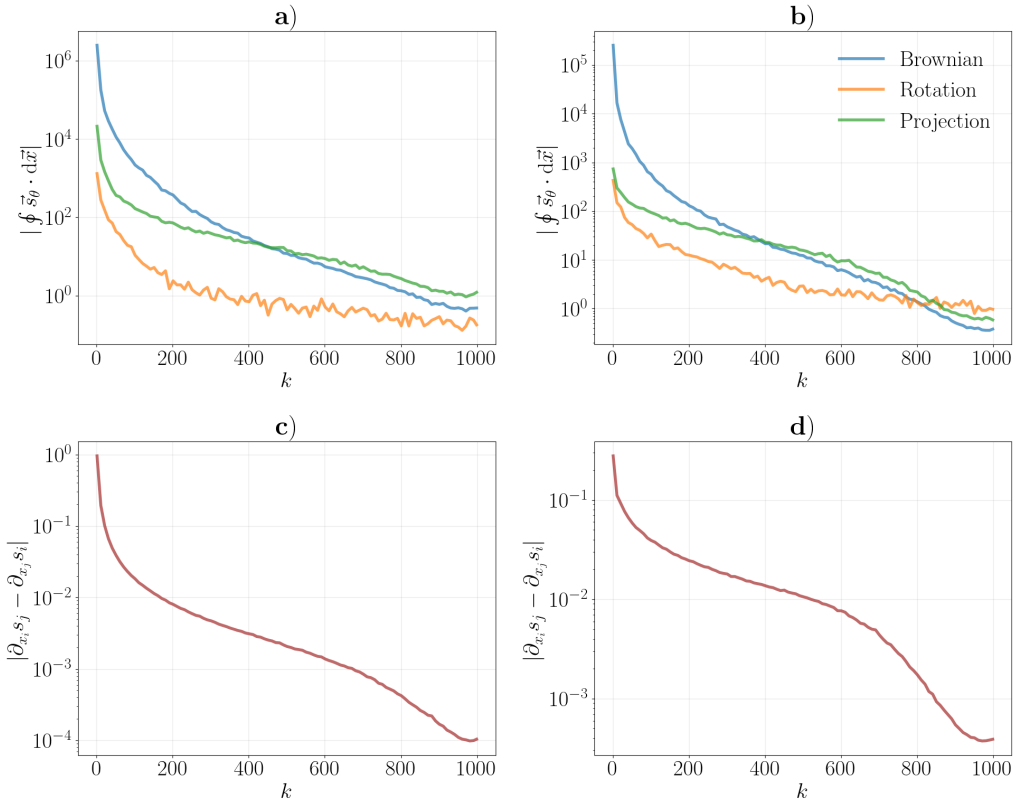


Figure 7: (CIFAR-10) Results of integral and differential constraints, as functions of discrete time index k : **a)** shows the absolute value of the integral condition $\oint \vec{s}_\theta \cdot d\vec{x}$; **b)** presents the same quantity but for the latent dynamics; **c)** reports the differential condition $|\partial_{x_i} s_j - \partial_{x_j} s_i|$ in normal diffusion; **d)** shows the corresponding differential condition in latent diffusion.

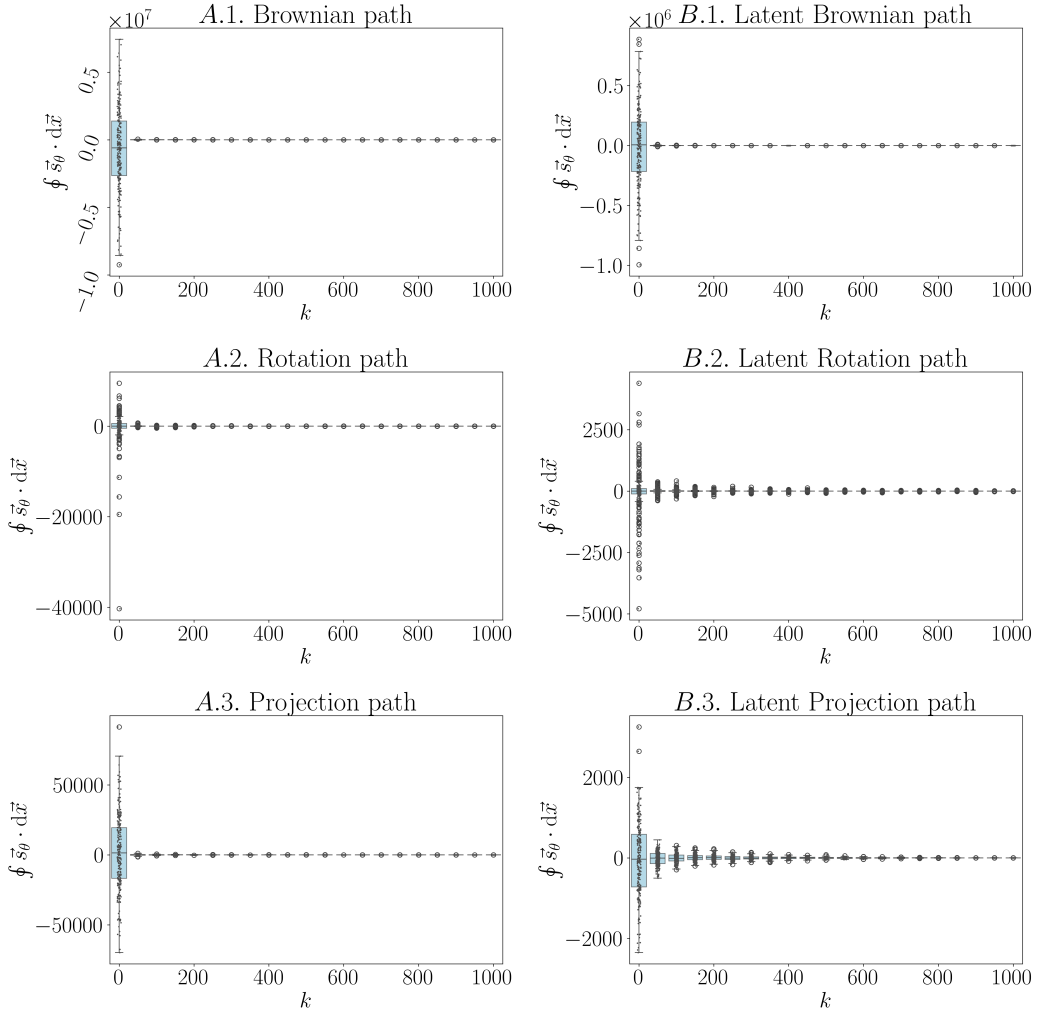


Figure 8: (CIFAR-10) Summary statistics of $\oint \vec{s}_\theta \cdot d\vec{x}$ calculated by different path-generating mechanisms, in normal and latent diffusions.

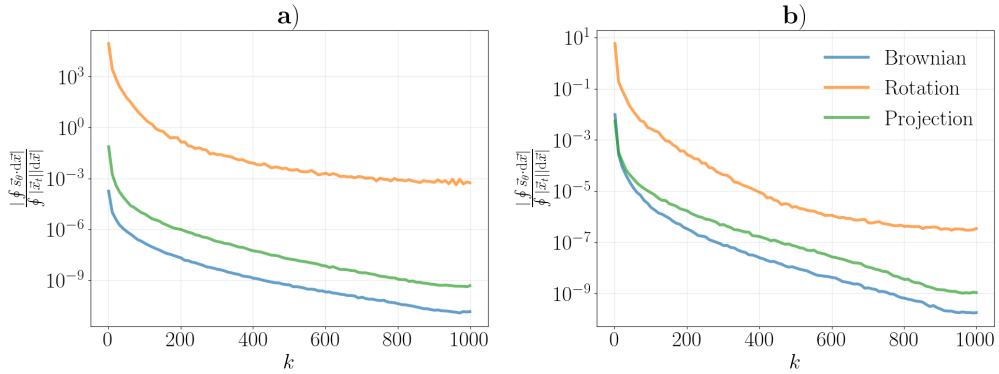


Figure 9: (CIFAR-10) Results of integral constraints, as functions of discrete time index k : **a**) shows the absolute value of the integral condition $\oint \vec{s}_\theta \cdot d\vec{x}$ normalized by the path length and the strength of the deterministic flow, $\oint |\vec{x}_t| ||d\vec{x}||$; **b**) presents the same quantity but for the latent dynamics.

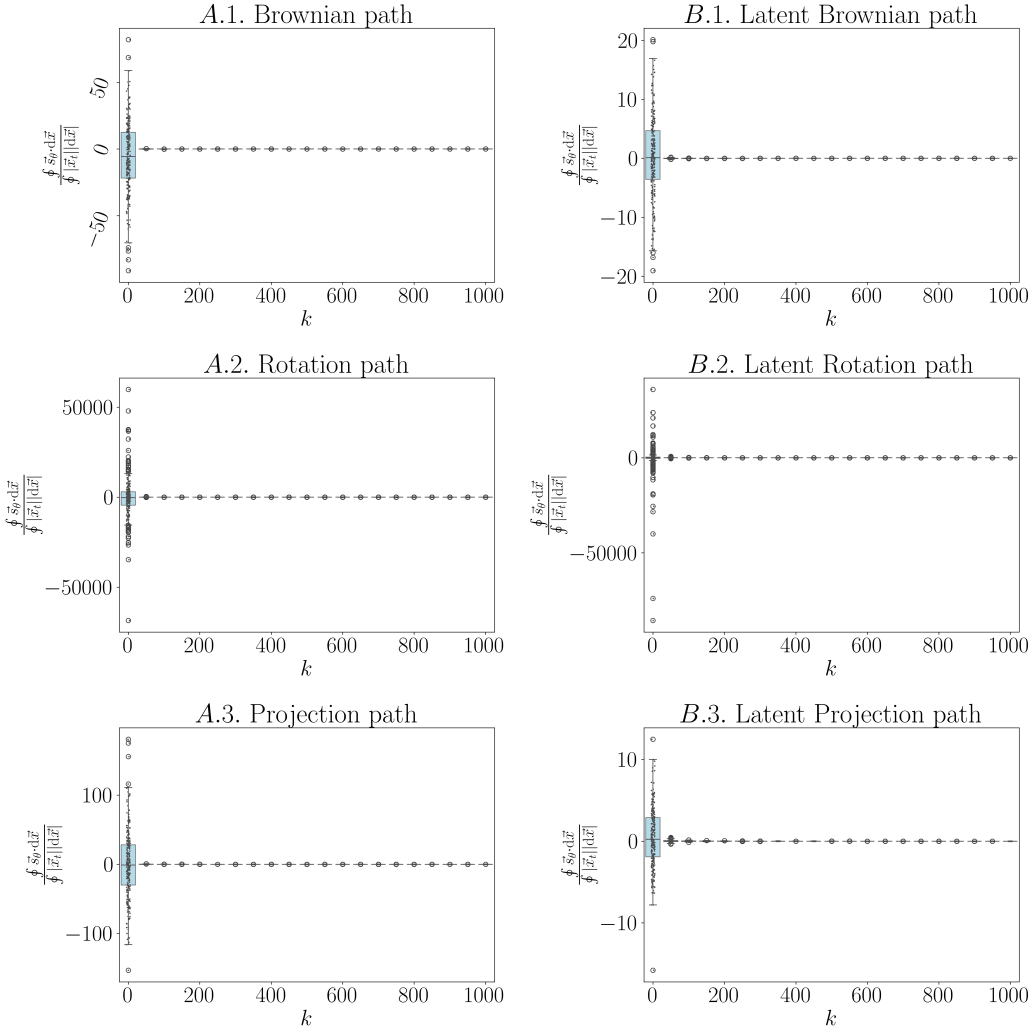


Figure 10: (CIFAR-10) Summary statistics of $|\oint \vec{s}_\theta \cdot d\vec{x}| \oint |\vec{x}_t| |d\vec{x}|$ calculated by different path-generating mechanisms, in normal and latent diffusions.